Mon. Not. R. astr. Soc. (1982) **198**, 91–110

Observations of the spectra of Q0122 – 380 and Q1101 – 264

R. F. Carswell and J. A. J. Whelan *Institute of Astronomy, Madingley Road, Cambridge CB3 0HA*

Malcolm G. Smith★ *Anglo-Australian Observatory, PO Box 296, Epping, NSW 2121, Australia*

A. Boksenberg and David Tytler *Department of Physics and Astronomy, University College London, Gower Street, London WC1E 6BT*

Received 1981 March 16; in original form 1980 July 31

Summary. The spectra of the QSOs Q0122 – 380 (z_{em} = 2.181) and Q1101 – 264 (z_{em} = 2.143) are described and discussed. Wavelengths and equivalent widths for the absorption lines in the range 3200–5200 Å are given for each object, and a number of absorption systems are suggested. Evidence is presented for velocity structure in some of these systems. We draw attention to the biasses and errors in continuum fitting, and their effect on the measured equivalent widths of the absorption lines. The Lyα absorption line densities in these and other QSOs are compared. It is found that in a single QSO the absorption line density appears to increase with decreasing observed wavelength (or absorption redshift). In contrast, from QSO to QSO there is a small increase in mean line density with QSO emission (or mean absorption) redshift. Some systematic effects may account for this difference, and for the small data sample available the density function is consistent with that expected from a uniform space distribution of comoving absorbers.

1 Introduction

In order to understand the nature and origin of narrow absorption lines in QSO spectra and to discover how the number of these lines varies with emission redshift and other parameters it is necessary to obtain high signal-to-noise data with the same absorption line detection sensitivity for a large sample of QSOs. Such a study will be statistical in nature and it is important to consider a QSO sample selected without bias arising from the presence of the absorption lines themselves. The sample of optically selected high-redshift QSOs detected by slitless spectroscopy (Smith 1975, 1976, 1978) has made available a large sample of objects for more detailed study. Unless there is a high absorption line density in the emission lines,

★ Present address: Royal Observatory, Blackford Hill, Edinburgh EH9 3HJ.

the presence of narrow absorption features will not significantly affect the discovery of the QSOs at the very low spectral resolution used.

We have undertaken a spectroscopic survey at intermediate resolution and relatively high signal-to-noise ratio of a sample of optically selected QSOs to investigate the properties of the narrow absorption lines. Previously we have described the $z_{em} = 2.22$ QSO Q1246 – 057 (Boksenberg *et al.* 1978) and here we describe two further objects of similar redshift Q0122 – 380 ($z_{em} = 2.18$; Osmer & Smith 1977b) and Q1101 – 264 ($z_{em} = 2.14$; Osmer & Smith 1977a). Related work on PKS 2126 – 158, Q0453 – 423 and Q0002 – 422 has been described by Young *et al.* (1979) and Sargent *et al.* (1979).

2 Observations

Spectroscopic observations of Q0122 – 380 and Q1101 – 264 were obtained with the Image Photon Counting System (IPCS) mounted on the RGO spectrograph at the $f/8$ focus of the Anglo-Australian Telescope. A grating giving a reciprocal dispersion of 34 Å mm^{-1} was used. The channel size along the dispersion was ~ 15 μm, corresponding to 0.5 Å; the projected slit width was ~ three channels giving an effective resolution allowing for data rebinning of 1.5–2 Å. The exposure times and wavelength regions covered are given in Table 1 where 1D and 2D refer to the mode of data recording. In the one-dimensional (1D) mode the data were recorded in 2048 channels along the dispersion through two (star and sky) spectrograph apertures. The positions of star and sky were swapped at intervals of typically 1000 s to allow for differences in system response when subtracting the sky component. In the two-dimensional mode (2D) the data were recorded in 1750 channels along the dispersion by nine increments along the slit each separated by ~ 3 arcsec. The object spectrum was recorded in two or three of the increments, the rest containing the sky signal. The object spectrum was recorded in two different sets of increments so that system response differences could be removed.

Exposures of an argon comparison lamp spectrum were obtained usually every 1000 s to monitor small system wavelength drifts and to allow these to be removed in the final data analysis. In some circumstances drifts up to 20 μm (~ 0.7 Å) were found during an integration. We determined the wavelength scale from an average of the arcs taken just before and just after each individual run. Allowing for weighting of individual runs in producing the final spectrum, the spectrum wavelength error is $\lesssim 0.2$ Å.

The system response function was determined by using Oke's (1974) spectrophotometry of standard stars which were observed at each wavelength setting through neutral density filters. The QSO spectra were corrected to an approximate relative scale of photon s^{-1} Å^{-1} ($\propto \nu f_\nu$) and rebinned to a constant channel size of 0.5 Å. Since conditions during observa-

Table 1. Observations.

Object	Position (1950.0) RA	Position (1950.0) Dec	Date (UT)	Wavelength region (A)	Total Integration time (sec)	Comments
Q0122-380	$01^h22^m02^s.1$	$-38°00'01''$	1977 September 15.60	4060–5040	12000	1D
			16.50	4270–5260	11500	1D
			October 13.58	3200–3900	14000	1D
			14.50	4060–5040	6000	1D, some cloud
			1978 September 25.71	3300–4100	9300	1D
Q1101-264	$11^h00^m59^s.7$	$-26°29'05''$	1977 March 28.49	3640–4520	6000	2D
			28.56	4500–5380	3500	2D - No standard star
			28.64	3175–4000	6000	2D

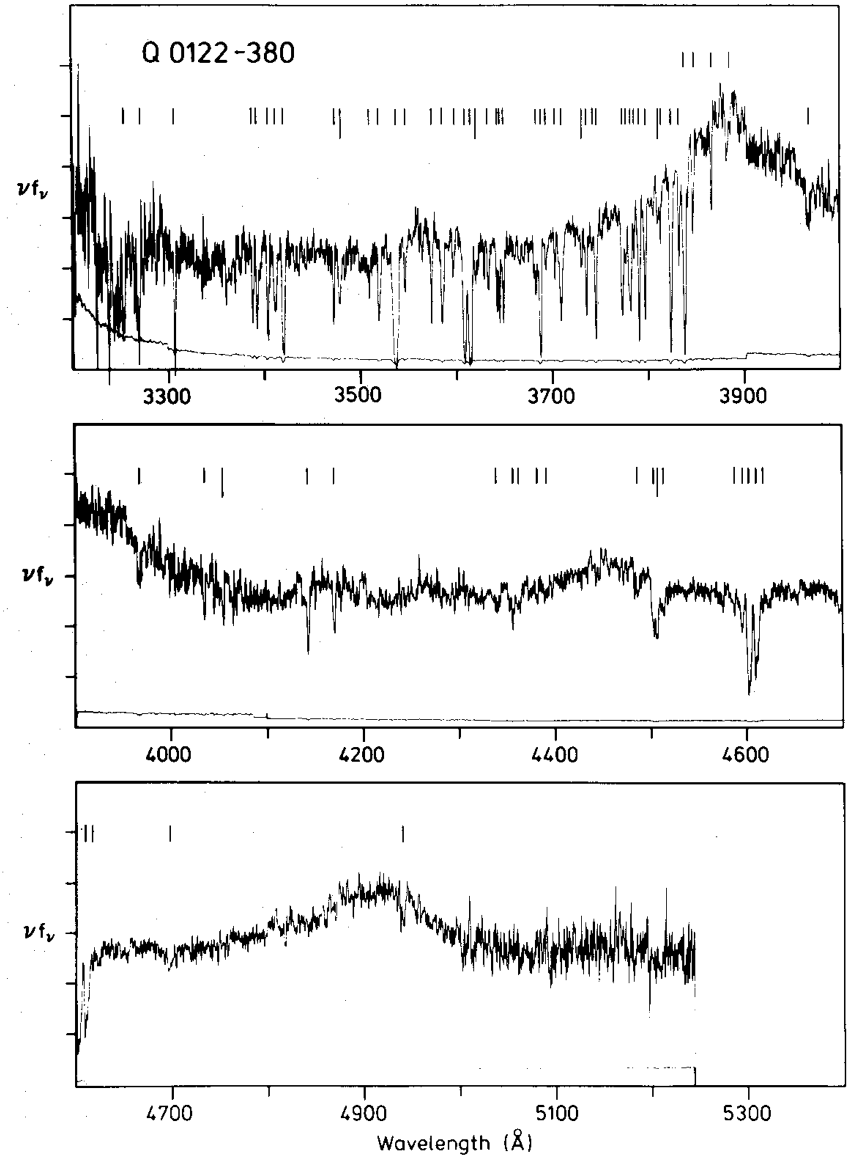

Figure 1. The spectrum of Q0122 – 380 obtained from the summation of the IPCS data. The lower curve shows the 1σ error level.

tions were generally not photometric we have made no attempt to correct to an absolute flux scale.

The individual runs were summed using weighting factors appropriate to the noise levels determined individually for each channel, so as to minimize the resultant variance in the final reduced spectrum.

The resultant spectra of Q0122 – 380 and Q1101 – 264 are shown in Figs 1 and 2. The lower curve is the 1σ error in each rebinned channel.

3 Emission line spectra

The presence of strong absorption lines over most of the range of our spectra makes a detailed emission line study difficult. The profiles of Lyα and any lines at shorter wavelengths are likely to be severely affected. Also, because a narrow slit was used the spectra cannot be used to determine relative fluxes. However, the high signal-to-noise ratio and high

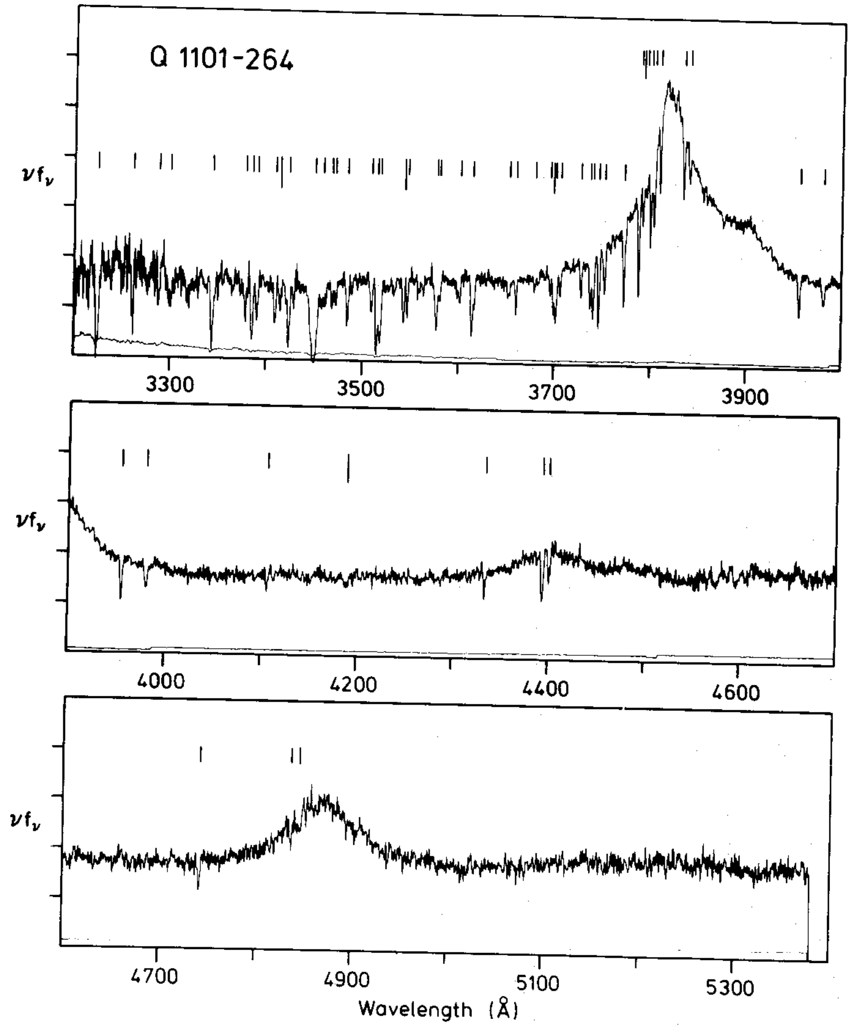

Figure 2. The spectrum of Q1101 – 264.

resolution make it possible to detect weak emission lines, even in those parts of the spectrum strongly affected by absorption lines. The emission lines found, and estimates of their equivalent widths, are given in Table 2.

For Q1101 – 264 our values for the strong lines are in reasonable agreement with those found by Osmer & Smith (1977a), though the Lyα equivalent width is somewhat higher since we have allowed for the absorption lines we have found in our spectra. We have also attempted to deconvolve the Lyα + N v λ1240 profile into its components, assuming that the profiles are symmetric. The apparent symmetry of the C IV λ1549 emission line suggests that this is a reasonable procedure. Wills & Netzer (1979) have suggested that O IV] λ1402 generally dominates Si IV λ1397, but in this case we find that an equal mixture gives good redshift agreement with other lines. There is a second component to this feature at a rest wavelength of about 1427 Å which has not been seen in other QSOs previously (see Baldwin & Netzer 1978) and which we have not been able to identify.

Q0122 – 380 has a richer emission line spectrum, even though the lines are rather broader and close components (such as Lyα and N v λ1240) have merged to the extent that they are no longer separable. The C IV λ1549 line-profile (at 4915 Å) looks asymmetric. In the limited wavelength range observed we have detected lines we identify with Lyα (+ N v λ1240), O I λ1303, C II λ1335, Si IV + O IV] λ1400 and C IV λ1549. The C II λ1335 line in particular

Table 2. Emission lines.

λ_{vac}	ID	z	EW(rest)	Comments
Q0122-380. z = 2.181				
3565:	1120?	-	3	Clearly present on two separate spectra
3877	Lyα & NV 1240	2.189	55	z from identifying line peak with Lyα
4165:	OI 1303	2.196	3	
4288:	CII 1335	2.212	2	
4461	SiIV 1397 OIV 1402	2.193 2.182	9	
4915	CIV 1549	2.173	22:	Continuum uncertain
Q01101-264. z = 2.143				
3255:	OVI 1034	2.148	-	Continuum uncertain
3818	Lyα	2.141	73	
3907	NV 1240	2.151	6	Wavelength uncertain
4401	SiIV 1397 OIV 1402	2.150 2.139	8	
4488:	1427?	-	2	
4872	CIV 1549	2.145	21	

appears to be stronger than in the objects studied by Baldwin & Netzer (1978), though it is possible that it might not have been detected at their lower resolution.

In addition an unidentified line is present at about 1120 Å – the precise wavelength is difficult to determine because of the presence of strong absorption lines. Possible identifications are Si II λλ1122, 1128 or multiplet 1 of Fe III, though the wavelength agreement is not very good in either case. Finally, we note that though the results obtained by Osmer & Smith (1977b) are consistent with our much better data reported here, their claim that Lyα emission is weak relative to N V λ1240 is not correct.

4 Absorption line spectra

To compare properly absorption lines in one QSO with those in another it is necessary to demand that all the lines involved in the comparison are subject to the same detectability limit. This can be ensured by comparing only observations obtained at the same spectral resolution and at the same signal-to-noise ratio. The former requirement is satisifed by using the same instrument system. The latter requirement is difficult to fulfil *a priori* at the telescope due to the many variables involved. However, it can be ensured in the data analysis by having an absorption line finding procedure which allows an equivalent width limit, W_λ, to be set such that: (a) no sharp lines with larger equivalent width will be missed; (b) very few, if any, spurious lines will be included. Such a procedure has been described in detail by Young *et al.* (1979, IIc). The technique used here is similar except in the determination of the continuum.

There are a number of possible methods for continuum fitting. The most direct method is to form a local average over a number of data points, then to see if any of the data points involved depart significantly from that determined mean. If the fluctuations about the mean are within the expected statistical errors then that region of the spectrum is, as far as we can tell, free of emission and absorption features. The mean count level across the whole of the region is then used to give a single value for the continuum level at the central wavelength for this region. If, however, the fluctuations from the mean are deemed significant, the whole region is ignored. There may be weak lines which can not detect at our signal-to-noise ratio which could bias the results, but this is largely unavoidable given any local technique for determining the continuum level.

The continuum for the whole spectrum is then obtained by interpolating over the whole spectrum, and smoothing if necessary.

Typically we found that 15–25 data points (of 0.5 Å each) served well for the averaging process, and an acceptable continuum level was determined (after rejecting the highest and lowest points to allow for the very occasional 'fly' point) if all residuals were less than 1.5–2σ from the local mean. Given this, it is possible to determine a formal error for the continuum level, and this is usually $\leqslant 2$ per cent for the two QSOs described in this paper except in the part of the spectrum below 3400 Å where the signal-to-noise ratio is relatively low. However, near emission lines such as Lyα the method tended to break down, mainly because of the sharp gradients in the spectrum. Generally, in regions of very high line density the continuum is determined by rather few values – the direct method works best where it is least needed, in those regions with few features. This will affect results for higher line densities but did not significantly affect the analysis of the spectra of the two QSOs described here.

In strong emission lines where the direct method failed a 'one sided' distribution technique was used. Here the method was to average over, say 50–75 data points, throw away all values less than 2σ below the computer average and compute a new average iteratively, terminating the process after a few iterations (normally three would suffice). While it is not necessarily true that a continuum derived by this method would agree with that from the direct approach, or, indeed, with reality, in fact for the parameters used there was final agreement to 5 per cent or better where tests were made, though since continuum estimation remains largely subjective in strong emission lines, the final check of 'goodness of fit' was always made by eye. The results of continuum fitting by this method also agreed well with those from using the two-sided technique described by Young *et al.* (1979).

Having obtained the continuum level, the absorption line lists of Tables 3 and 4 were generated for Q0122 – 380 and Q1101 – 264. A candidate line was regarded as real if its equivalent width (W) was over four times the error due to counting statistics determined over the line width, $\sigma(W)$. From trials on flat field data it appears that a line could be regarded as certain at this level. This apparently very conservative value is required because the absorption lines are about 10 channels wide at the continuum, and consequently $\sigma(W)$ can not be directly equated with that for a normal distribution because of the large number of degrees of freedom. In addition there are small variations in the instrument response which could not be removed, and the line detection significance level is a sensitive function of the continuum level which is itself not always well determined. The error $\sigma(W)$ given in Tables 3 and 4 is due to counting statistics only and does not include that due to continuum uncertainty.

The effects of continuum uncertainty on the line equivalent widths can be estimated *approximately* from fairly simple considerations. Suppose, for the moment, that near the continuum level the absorption line has vertical sides. Then, if the continuum estimate is in error by a factor $1+\epsilon$ (i.e. $N' = N(1+\epsilon)$), the measured equivalent width W' will be related to the true equivalent width W by

$$W' = \frac{1}{1+\epsilon}\,\{W + M_{\mathrm{L}}\,\epsilon\},$$

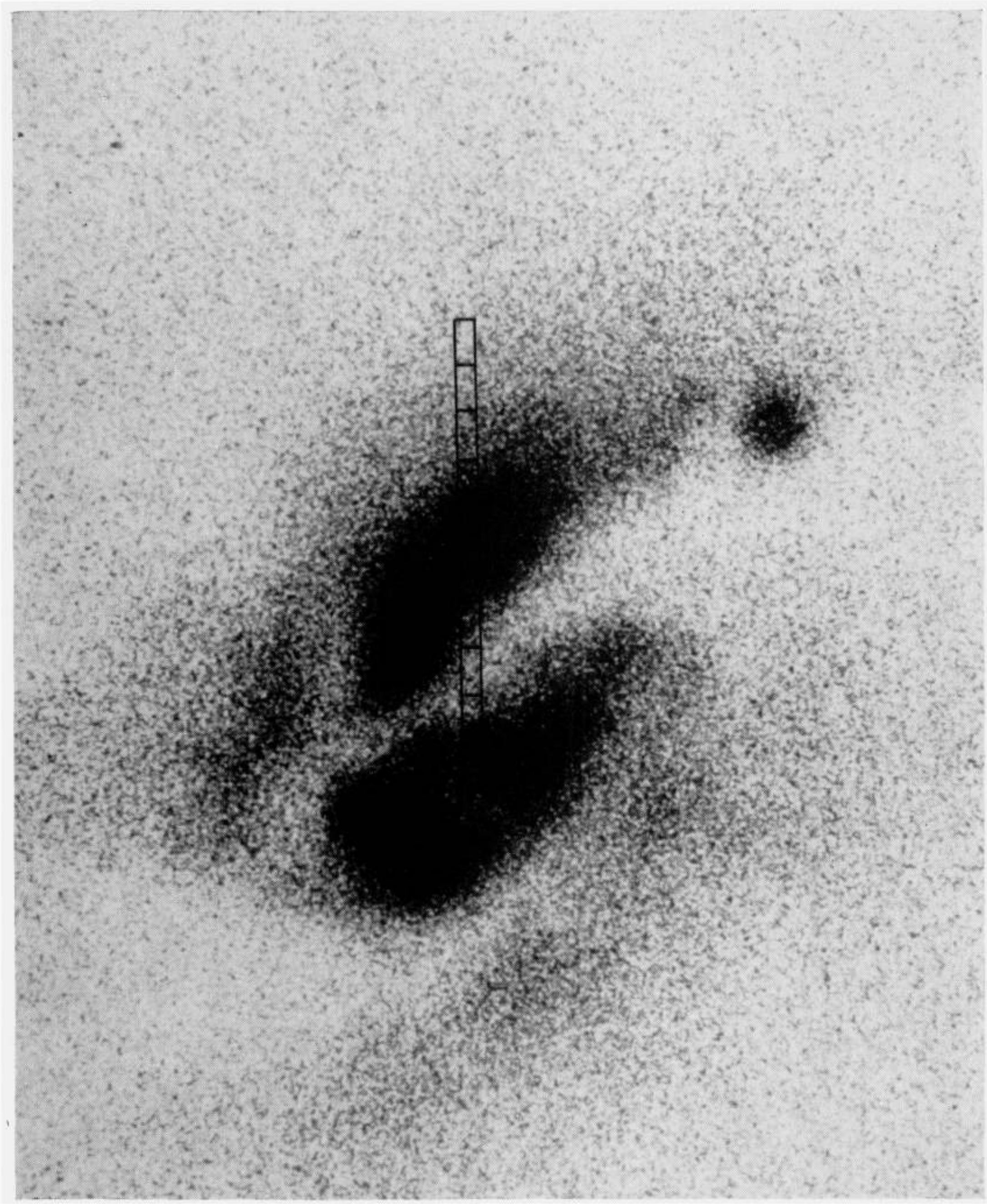

Plate 1. Ultraviolet exposure of the nucleus of NGC 1365 showing configuration of the slit. North is up and east to the right. The increments are numbered 1 to 10, going from north to south, and the Seyfert nucleus is in increment 9. Slit dimensions are 27×1.2 arsec. The clump to the west of the southern tip of our slit corresponds to the two southern 'hot spots' shown in Fig. 1. (From a Mount Stromlo and Siding Spring Observatories 1-m Richey Chrétien plate, kindly supplied to us by A. Duus.)

[*facing page* 1097]

Table 3. Absorption lines in Q0122 – 380.

n	λ^{+}_{obs}	λ^{+}_{vac}	σ	EW	σ		Comments
1	3254.01	3254.95	0.28	1.88	0.40		Noisy region of spectrum
2	3269.61	3270.55	0.23	2.25	0.40		
3	3306.52	3307.47	0.18	2.07	0.28		
4	3388.24	3389.21	0.09	1.11	0.15		
5	3393.55	3394.52	0.14	1.75	0.19		
6	3404.01	3404.98	0.07	1.73	0.13		
7	3411.63	3412.60	0.30	1.81	0.21	*	
8	3420.24	3421.22	0.11	2.84	0.16	*	
9	3472.17	3473.16	0.10	1.13	0.13		
10	3478.81	3479.81	0.25	1.47	0.17		
11	3506.74	3507.74	0.47	1.72	0.23		Broad (∿12A) noisy feature
12	3519.94	3520.95	0.12	1.72	0.15		
13	3536.52	3537.53	0.10	6.30	0.17		
14	3547.08	3548.10	0.15	0.91	0.13		
15	3574.19	3575.20	0.10	1.25	0.11		
16	3585.60	3586.62	0.18	2.22	0.14		
17	3597.23	3598.26	0.09	0.51	0.09		
18	3608.79	3609.82	0.08	3.69	0.11	*	
19	3614.53	3615.56	0.07	4.41	0.11	*	
20	3621.07	3622.10	0.21	0.90	0.12	*	
21	3633.72	3634.75	0.07	0.72	0.09		
22	3642.72	3643.75	0.10	0.77	0.08	*	
23	3645.44	3646.48	0.11	0.99	0.09	*	
24	3649.24	3650.28	0.10	1.04	0.09	*	
25	3682.80	3683.85	0.17	1.16	0.12	*	
26	3687.85	3688.90	0.07	2.69	0.09	*	
27	3694.04	3695.09	0.23	0.59	0.12		
28	3703.13	3704.18	0.19	0.45	0.08		
29	3709.47	3710.53	0.14	2.39	0.13		Resolved
30	3730.78	3731.84	0.24	0.66	0.10	*	
31	3736.06	3737.13	0.15	1.43	0.11	*	
32	3741.76	3742.83	0.21	0.36	0.08	*	
33	3745.96	3747.02	0.11	2.02	0.10	*	
34	3773.78	3774.85	0.09	2.06	0.09	*	
35	3777.21	3778.28	0.09	0.41	0.05	*	
36	3781.36	3782.43	0.10	2.26	0.09	*	
37	3785.57	3786.64	0.11	0.41	0.06	*	

4

Table 3. – *continued*

n	λ^{+}_{obs}	λ^{+}_{vac}	σ	EW	σ		Comments
38	3790.98	3792.06	0.07	1.88	0.08		
39	3797.27	3798.34	0.08	1.47	0.08		
40	3810.44	3811.52	0.13	0.30	0.05	*	
41	3813.19	3814.27	0.16	0.49	0.07	*	
42	3824.27	3825.35	0.09	2.74	0.09		
43	3832.67	3833.75	0.12	1.01	0.07	*	
44	3838.44	3839.52	0.09	3.54	0.08	*	
45	3847.11	3848.20	0.07	0.73	0.06		
46	3866.20	3867.29	0.10	0.74	0.07		
47	3883.43	3884.53	0.15	0.61	0.07		
48	3967.66	3968.78	0.21	0.90	0.13		
49	4034.97	4036.11	0.16	0.59	0.13		
50	4054.85	4056.00	0.22	0.62	0.12		
51	4142.18	4143.34	0.16	1.59	0.13		
52	4170.15	4171.32	0.21	1.00	0.12		
53	4340.95	4342.16	0.25	0.66	0.08		
54	4355.92	4357.14	0.23	1.19	0.10	*	
55	4363.99	4364.21	0.23	0.73	0.10	*	
56	4381.96	4383.18	0.08	0.28	0.06		May be further structure in blue wing
57	4390.88	4392.11	0.35	0.46	0.09		Messy feature
58	4486.26	44.87.52	0.19	0.62	0.08		
59	4503.21	4504.47	0.09	1.14	0.06	*	
60	4507.30	4508.56	0.09	1.47	0.07	*	
61	4513.29	4514.55	0.17	1.03	0.08	*	
62	4587.22	4588.50	0.18	0.38	0.08		
63	4595.46	4596.74	0.24	1.14	0.10	*	
64	4603.36	4604.65	0.09	3.69	0.09	*	
65	4611.09	4612.38	0.09	2.97	0.10	*	
66	4617.43	4618.72	0.19	0.27	0.06	*	
67	4698.07	4699.39	0.28	0.58	0.10		
68	4940.30	4941.68	0.18	0.68	0.08		

* Blended line - wavelength and equivalent width less certain.

\+ Heliocentric wavelengths.

where M_L is the total zero intensity line width. Thus

$$\frac{W'}{W} \simeq 1 + (M_L/W - 1)\epsilon$$

for small ϵ.

If allowance is made for the fact that line profiles are not vertical sided, then for $\epsilon > 0$ the correction derived here is an underestimate, and for $\epsilon < 0$ the magnitude of the change is overestimated. When the continuum height is overestimated over the entire wavelength range then the measured equivalent width can appear to be indefinitely large. In practice we are saved from this catastrophe by having finite signal-to-noise ratio; a line may be deemed to be bounded where, say, two channels together are higher than the assumed continuum level (as was done here).

The widths of the weaker lines at the continuum ($\lesssim 2.5$ Å equivalent width) are usually found to be of order 5–6 Å, though there is considerable scatter in this quantity. Thus, for a 2 per cent continuum error, we estimate there will be an uncertainty in equivalent width ~ 0.1 Å for these lines. This agrees well with an error estimate obtained by artificially changing the continuum level by 2 per cent and redetermining the line equivalent widths using the original QSO spectral data.

Since the direct continuum fitting procedure is not 'one-sided', it should be free from most sources of bias. However, there remains the possibility that weak undetected absorption lines may systematically bias the continuum estimate below the real value, and, if the equivalent width distribution function is constant (to within a normalization factor), this could become more serious a problem as the line density increases. That the procedure works at all is an indication that either such weak lines are insignificant, or they are distributed remarkably densely and uniformly with wavelength. An independent check for such bias for Q1101 – 264 was made by intercomparison of the equivalent widths of the absorptions lines determined from higher resolution data (Carswell *et al.*, in preparation) with those given here, and none was found. For high redshift QSOs, such as Q0420 – 388 ($z_{em} = 3.12$; Hewer *et al.*, in preparation, see also Smith *et al.* 1981), and PKS 2126 – 15 ($z_{em} = 3.27$, Young *et al.* 1979), the direct method fails to find enough line-free regions reliably to estimate the continuum. This indicates that the total absorption line density may be somewhat higher in these objects, but does not give us a quantitative estimate of this density. Under these circumstances there is the strong possibility that the one-sided method may underestimate the continuum, and so the equivalent widths of the absorption lines may by systematically low.

The mean wavelength error for each line in Tables 3 and 4 can be determined using the procedure of Young *et al.* (1979). The total error in the wavelength, $\sigma(\lambda)$ is given by

$$\sigma(\lambda) = \sqrt{\sigma_c^2 + \sigma_F^2},$$

where σ_F is the uncertainty determined from the arc fitting procedure and σ_c is the error due to counting statistics given approximately by

$$\sigma_c \sim \frac{\sigma(W)}{W} \frac{M_L}{\sqrt{12}}$$

where M_L is the total zero intensity line width.

Some candidate lines show more than one minimum suggesting that they may be just resolved at our resolution. To examine these lines a running average over three channels (corresponding to the estimated resolution element) was computed for the line and minima and maxima found. Local maximum points were deemed to divide components. The component by component line significance was evaluated and such components were included in Tables 3 and 4 if they individually satisfied the line reality critiera. In cases where no separable components satisfied the existence criteria the line is noted as being broad and resolved. The method is suspect for strong broader lines with essentially zero

Table 4. Absorption lines in Q1101 − 264.

n	λ^{+}_{obs}	λ^{+}_{vac}	σ	EW	σ		Comments
1	3224.60	3225.53	0.20	3.50	(0.31)		Noisy spectrum, continuum uncertain
2	3260.91	3261.85	0.14	1.53	(0.22)		" " " "
3	3288.18	3289.13	0.14	0.89	(0.18)		Continuum uncertain
4	3299.79	3300.74	0.23	0.84	(0.19)		Probably resolved; continuum uncertain
5	3343.95	3344.91	0.13	2.61	0.18		
6	3377.94	3378.91	0.23	1.23	0.17		
7	3385.27	3386.24	0.14	2.12	0.16		
8	3390.45	3391.42	0.20	1.17	0.15		
9	3409.14	3410.12	0.11	1.26	0.13		
10	3414.41	3415.39	0.19	0.71	0.14		
11	3423.39	3424.37	0.11	2.05	0.12		
12	3449.48	3450.47	0.13	8.06	0.20	*	Broad line, central intensity ~ zero
13	3459.21	3460.20	0.30	1.58	0.17	*	Resolved
14	3468.36	3469.35	0.22	0.61	0.11	*	
15	3471.90	3472.91	0.25	0.76	0.11	*	
16	3484.52	3485.52	0.12	1.29	0.13		
17	3509.49	3510.49	0.22	0.93	0.12		
18	3515.17	3516.17	0.09	2.22	0.09	*	
19	3518.64	3519.64	0.09	2.46	0.09	*	
20	3542.92	3543.93	0.14	1.19	0.11	*	
21	3547.00	3548.01	0.15	0.73	0.10	*	
22	3577.01	3578.03	0.13	1.97	0.11		
23	3580.98	3582.00	0.18	0.57	0.08		
24	3600.50	3601.52	0.18	0.93	0.11		Possibly resolved
25	3614.89	3615.92	0.10	2.38	0.10		
26	3652.59	3653.63	0.21	0.68	0.09		
27	3660.06	3661.10	0.10	0.70	0.06		
28	3679.55	3680.60	0.13	0.30	0.06		
29	3695.58	3696.63	0.15	0.58	0.06	*	
30	3699.00	3700.05	0.09	0.91	0.05	*	
31	3701.77	3702.82	0.09	1.47	0.05	*	
32	3706.13	3707.18	0.17	0.64	0.06	*	
33	3727.69	3728.75	0.09	0.66	0.05		
34	3737.21	3738.28	0.10	1.06	0.05	*	
35	3740.49	3741.56	0.08	1.44	0.05	*	
36	3746.30	3747.37	0.08	1.39	0.05		
37	3752.21	3753.28	0,09	0.96	0.05		
38	3772.36	3773.43	0.09	1.36	0.04		

Table 4. – *continued*

n	λ^{+}_{obs}	λ^{+}_{vac}	σ	EW	σ		Comments
39	3787.49	3788.56	0.09	1.32	(0.04)	*	In blue wing Lyα emission line
40	3792.09	3793.16	0.11	0.50	(0.03)	*	" " " " " "
41	3795.61	3796.69	0.11	0.31	(0.03)	*	Marginal line, depends critically on assumed continuum level
42	3799.52	3800.60	0.08	0.92	(0.03)	*	In blue wing Lyα emission line
43	3803.32	3804.40	0.09	1.07	(0.04)	*	" " " " " "
44	3809.16	3810.24	0.09	0.46	(0.03)	*	" " " " " "
45	3833.54	3834.63	0.10	0.61	0.03		In red wing Lyα emission line
46	3839.78	3840.87	0.08	0.26	0.03		" " " " " "
47	3955.27	3956.39	0.09	1.11	0.05		
48	3980.83	3981.95	0.13	0.83	0.05		
49	4106.35	4107.50	0.13	0.40	0.08		
50	4188.63	4189.80	0.34	0.53	0.11		Broad (~6A) shallow feature
51	4333.48	4334.70	0.13	0.66	0.08		
52	4393.48	4394.71	0.11	1.37	0.07		
53	4400.52	4401.75	0.11	0.73	0.07		
54	4741.85	4743.17	0.14	0.83	0.11		
55	4836.72	4838.06	0.19	0.32	0.08		
56	4844.96	4846.30	0.37	0.41	0.10		

* Blended line – wavelength and equivalent width less certain.

\+ Heliocentric wavelengths.

residual intensity (usually subsequently identified as Lyα in a strong system) and may give more resolved components than are present. Under these circumstances the entire range with zero intensity was included in a single line.

Other uncertainties include blended lines, and the shape of the intrinsic emission-line profiles (from which absorption occurs); in such regions the equivalent widths of Tables 3 and 4 are very uncertain.

The line lists of Tables 3 and 4 depend on the *local* signal-to-noise ratio and are *not* ones which contain all lines complete to some uniform equivalent width, for example. The completeness limit for an isolated feature may be estimated conservatively as about $5\sigma(W)$.

None of these uncertainties are likely to be very serious when intercomparing QSO spectra if the data obtained is of nearly uniform signal-to-noise ratio, the redshifts are similar, and emission line regions of the spectra are avoided. Because of this we believe that the material described here forms a useful basis for comparative studies of the properties of absorption-line QSOs. For disparate redshifts this relatively simple approach may be inadequate, with uncertainty in the continuum level providing the main source of error. These points are being investigated further by one of us (DRT).

5 Absorption redshift systems

We have determined possible absorption redshift systems for the two QSOs, and give details of these in Tables 5 and 6. *f* values are from Morton (1978). Automatic methods for finding

Table 5. Absorption redshift systems in Q0122 – 380.

λ_{vac}	σ	EW	σ	ID		f	z	Comments	
Z = 1.97 Complex									
		z = 1.9638							
3575.20	0.10	1.25	0.11	SiIII	1206.510	1.66	1.9633	Too strong?	
4588.50	0.18	0.38	0.08	CIV	1548.188	0.194	1.9638		
4596.74	0.24	1.14	0.10	CIV	1550.762	0.097	1.9642	Blend CIV 1548.19	z = 1.9694
		z = 1.9694							
3609.82	0.08	3.69	0.11	Lyα		0.416	1.9694		
4596.74	0.24	1.14	0.10	CIV	1548.188	0.194	1.9691	Blend CIV 1550.76	z = 1.9638
4604.65	0.09	3.69	0.09	CIV	1550.762	0.097	1.9693	Blend CIV 1548.19	z = 1.9734
		z = 1.9734							
3586.62	0.18	2.22	0.14	SiIII	1206.510	1.66	1.9727		
3615.56	0.07	4.41	0.11	Lyα		0.416	1.9741		
3683.85	0.17	1.16	0.12	NV	1238.808	0.152	1.9737		
3695.09	0.23	0.59	0.12	NV	1242.796	0.076	1.9732		
3968.78	0.21	0.90	0.13	CII	1334.532	0.118	1.9739		
4143.34	0.16	1.59	0.13	SiIV	1393.755	0.528	1.9728		
4171.32	0.21	1.00	0.12	SiIV	1402.770	0.262	1.9736		
4604.65	0.09	3.69	0.09	CIV	1548.188	0.194	1.9742	Blend CIV 1550.76	z = 1.9694
4612.38	0.09	2.97	0.10	CIV	1550.762	0.097	1.9743	Blend CIV 1548.19	z = 1.9790
		z = 1.9790							
3622.10	0.21	0.90	0.12	Lyα		0.416	1.9795		
4612.38	0.09	2.97	0.10	CIV	1548.188	0.194	1.9792	Blend CIV 1550.76	z = 1.9734
4618.72	0.19	0.27	0.06	CIV	1550.762	0.097	1.9784		
Z = 1.91 Systems									
		z = 1.9101							
3537.53	0.10	6.30	0.17	Lyα		0.416	1.9099		
3884.53	0.15	0.61	0.07	CII	1334.532	0.118	1.9108		
4056.00	0.22	0.62	0.12	SiIV	1393.755	0.528	1.9101		
4504.47	0.09	1.14	0.06	CIV	1548.188	0.194	1.9095		
4514.55	0.17	1.03	0.08	CIV	1550.762	0.097	1.9112	Blend CIV 1550.76	z = 1.9122
		z = 1.9122							
4508.56	0.09	1.47	0.07	CIV	1548.188	0.194	1.9122		
4514.55	0.17	1.03	0.08	CIV	1550.762	0.097	1.9112	Blend CIV 1550.76	z = 1.9101
		z = 1.8143							
3421.22	0.11	2.84	0.16	Lyα		0.416	1.8143		
4357.14	0.23	1.19	0.10	CIV	1548.188	0.194	1.8143		
4364.21	0.23	0.73	0.10	CIV	1550.762	0.097	1.8142		

absorption systems and assessing their significance have been described by Bahcall (1968), Coleman *et al.* (1976) and Young *et al.* (1979). In fact, the reality of most systems hinges mostly on their physical plausibility after wavelength agreement is found to be satisfactory, and on the detection of expected lines longward of the Lyα emission line. There are often problems arising because substructure in systems gives rise to rather poorer wavelength agreement than expected. A fully comprehensive procedure should take account not only of the relative line strengths within ionization stages, as does that of Young *et al.* (1979), but assess the likelihood of a given line being identified with an observed feature taking account of the observed line width. In the end these procedures tend to give candidate systems which are almost identical with those found, by a line pair search and requiring reasonable physical and

Table 6. Absorption redshift systems in Q1101 – 264.

n	λ_{vac}	σ	EW	σ	ID	f	z	Comments
			z = 1.8387					
6	3378.91	0.23	1.23	0.17	SiII 1190.416	0.251	1.8384	
7	3386.24	0.14	2.12	0.16	SiII 1193.289	0.500	1.8377	Possibly too strong - blended?
11	3424.37	0.11	2.05	0.12	SiIII 1206.510	1.66	1.8382	
12	3450.47	0.13	8.06	0.20	Ly α	0.416	1.8383	
22	3578.03	0.13	1.97	0.11	SiII 1260.421	0.959	1.8388	
29	3696.63	0.15	0.58	0.06	OI 1302.168	0.0486	1.8388	
31	3702.82	0.09	1.47	0.05	SiII 1304.372	0.147	1.8388	Too strong
39	3788.56	0.09	1.32	(0.04)	CII 1334.532	0.118	1.8389	
47	3956.39	0.09	1.11	0.05	SiIV 1393.755	0.528	1.8387	
48	3981.95	0.13	0.83	0.05	SiIV 1402.770	0.262	1.8386	
51	4334.70	0.13	0.66	0.08	SiII 1526.708	0.0764	1.8392	
52	4394.71	0.11	1.37	0.07	CIV 1548.188	0.194	1.8386	
53	4401.75	0.11	0.73	0.07	CIV 1550.762	0.097	1.8384	
54	4743.17	0.14	0.83	0.11	AlII 1670.787	1.88	1.8389	
			z = 1.4769					
(1	3225.53	0.20	3.50	(0.31)	OI 1302.168	0.0486	1.4770	Too strong? Ly α z = 1.6532)
(12	3450.47	0.13	8.06	0.20	SiIV 1393.755	0.528	1.4757	Ly α z = 1.8387, SiIV 1402 absent)
45	3834.63	0.10	0.61	0.03	CIV 1548.188	0.194	1.4769	
46	3840.87	0.08	0.26	0.03	CIV 1550.762	0.097	1.4768	
			z = 1.6532					
1	3225.53	0.20	3.50	(0.31)	Ly α	0.416	1.6533	
49	4107.50	0.13	0.40	0.08	CIV 1548.188	0.194	1.6531	
			z = 2.1250					
55	4838.06	0.19	0.32	0.08	CIV 1548.188	0.194	2.1250	
56	4846.30	0.37	0.41	0.10	CIV 1550.762	0.097	2.1251	

wavelength consistency, so in the absence of a satisfactory fully automatic method we have used this latter technique here.

Comments on the individual systems in each of the two objects follow:

Q0122 – 380 z_{em} = 2.181 (Table 5)

z_{abs} = *1.97 complex.* This complex appears to consist of at least four easily resolvable systems, with velocity separations of 570, 400 and 560 km s^{-1}. The most doubtful constituent is the z_{abs} = 1.9638 system, which is based on identifying the line at 4588.50 Å with C IV λ1548 only. The C IV λ1550 line is blended with C IV λ1548 from the z_{abs} = 1.9694 component, and Lyα is absent on our spectra. However, no other plausible identification was found for the feature, and its closeness to the C IV complex makes our proposed identification marginally more believable.

The strongest component at $z_{abs}=1.9734$ shows an interesting mixture of ionization states. In particular there is a plausible identification of N v λ1238, λ1242 in this system, so it may be one of those rare cases which show very high ionization with $z_{abs} \ll z_{em}$. For this system the C IV lines are resolved and the internal wavelength agreement is not very good, suggesting that at higher resolution we should see further velocity structure.

$z_{abs}=1.91$ *systems.* A pair of systems is present with velocity separation 215 km s^{-1}. Here one of the components is based on an apparent splitting of the C IV 1548 line. The C IV λ1550 line at 4514.55 Å appears to be resolved, but is too noisy to be certain of two components. The Lyα line at 3537.53 Å is also resolved, and could well arise from more than one component.

$z_{abs}=1.8143$. This system identifies a weak C IV doublet and a strong ultraviolet line as Lyα. No further plausible identifications were found.

These proposed systems identify only about one-third of the absorption lines we have found in the spectrum. It is usual to suppose that most of these are due to Lyα in weak systems with $z_{abs} \ll z_{em}$, following a suggestion first made by Lynds (1971). However, in Q0122 – 380 there are seven lines for which we have not found plausible systems at wavelengths greater than the Lyα emission line, an unusually large number. All of these are relatively weak, with observed equivalent widths less than 0.7 Å, but because of our strict criteria for inclusion in the line list few, it any, are likely to be spurious. The absorption analysis compares with that of PKS 0528 – 250, where Morton *et al.* (1980) have also found several unidentified absorption lines longward of the Lyα emission-line wavelength. Again these lines are relatively weak.

Q1101 – 264 $z_{em}=2.143$ *(Table 6)*

$z_{abs}=1.8387$. This is the only well-established redshift system in this object, with the usual lines characteristic of a medium-ionization system all present. The strongest absorption line in the observed spectrum is identified by Lyα at this redshift, and, while there appears to be some other component blended with some of the Si II lines, most of the lines appear unexceptional in strength. Most of the lines appear to be unresolved at the 2Å resolution used, but Lyα is broad and shows probable velocity structure.

$z_{abs}=1.4769$. This system provides the only reasonable identifications for the pair of lines in the long wavelength wing of the Lyα emission line, as the C IV doublet. No other plausible identifications were found. The suggested identification with O I λ1302 is much stronger than would be expected in the absence of C II λ1334 unless the system is very unusual, so it is rejected here.

$z_{abs}=1.6532$. The strong line at 3225.53 Å is identified at Lyα and a weak line at 4107.50 Å as C IV λ1548 in this possible system. Weak confirming evidence comes from the possible presence of a feature at $\lambda_{vac}=4114.6$ (EW = 0.25 Å) which would be identified with the weaker of the C IV pair, but this line did not satisfy our strict criteria for inclusion in the line list.

$z_{abs}=2.1250$. Again the tentative system is based only on the C IV doublet identifying a probable pair of lines in the short wavelength wing of the C IV emission line. Lyα appears not to be present in our spectrum at this redshift, though its expected position is in a crowded region in the Lyα emission line so it could well have been missed if it is fairly weak. No N v or Si IV absorption lines were found, so if this is a high-ionization system it is a weak-lined one.

We note that the only definite line longward of emission Lyα which remains unidentified is the broad feature at 4188.63 Å. We have found no plausible identification for this.

6 Column densities in the absorbing clouds

From the equivalent widths of the lines identified in each system we may estimate column densities for each of the ions using a variant of the doublet ratio method described by Strömgren (1948). This technique has been applied by a number of authors to interpret QSO absorption spectra, for example, Chan & Burbidge (1971), Carswell, Smith & Whelan (1977) and Sargent *et al.* (1979). However, as pointed out by Whelan, Smith & Carswell (1979), there are many uncertainties involved and the column densities derived can serve as only a rough guide. The difficulties arise from two sources:

First, the assumption that the velocity distribution within the clouds is Gaussian is not necessarily correct. Following the work Morton & Richstone (1973), Morton & Morton (1972), Boksenberg & Sargent (1975) and Boksenberg, Carswell & Sargent (1979), it appears that whenever moderately high resolution spectroscopy is attempted many lines are resolved into several components, each of which might possibly show differing relative ionization. This possibility makes the practice of applying a velocity dispersion parameter obtained from one ion to others extremely suspect.

Secondly, since the QSOs are invariably faint by stellar standards, the signal-to-noise ratio in the lines is relatively low, so line ratios are not well determined. Even if all the lines were isolated and had Gaussian profiles the errors often translate to a huge allowed range of column densities for a particular ion.

Because of these reservations we do not perform detailed abundance analyses, but in Table 7 we list ranges of column densities and velocity dispersion b-parameters* for selected multiplets where there is no evidence for blending or extended velocity structure. The range in these derived quantities is set by demanding that the predicted equivalent widths for all lines be within our formal 1σ error of the measured value.

It is evident that the range of velocity dispersion parameters allowed is quite large, and even so where it can be determined independently from more than one ion the agreement is not very good. The situation is worst for the system at $z_{abs} = 1.8387$ in Q1101 − 264, just that one which has sufficient lines that there would normally be some expectation of a good result. The Si II lines in this system are particularly interesting, given the uncertainties in the oscillator strengths that have been pointed out by Williams *et al.* (1975) and Morton (1978). Williams *et al.* suggest that Si II λ1304 must have a smaller f-value than Si II λ1526 on the basis of observations of the QSO 3C191, and Morton finds that Si II λ1526 is likely to have a larger f-value than generally accepted. From our data we find reasonable agreement if we suppose that both Si II λ1193 and λ1304 are blends with lines from some other redshift system. However, given the almost certain presence of unresolved velocity structure even this is not a good measure of the relative f-values.

Clearly, mean velocity dispersions could be determined from our data and applied to all the lines in the system to obtain column density estimates. However, given the poor internal agreement, this would be at best highly approximate and at worst misleading, and derivation of relative ionization and abundances requires data at improved resolution.

* The velocity distribution is assumed to have the form $\exp(-v^2/b^2)$.

Table 7. Column densities of selected ions.

λ_{vac}	EW_{obs}	σ	ID	f	b (km/s)	log N	b min	b max	log N min	log N max
Q 0122–380										
z = 1.9734										
3683.85	1.16	0.12	NV 1238	0.152	≳ 100	14.3	45	∞	14.3	14.5
3695.09	0.59	0.12	NV 1242	0.076						
4143.34	1.59	0.13	SiIV 1393	0.528	65	14.0	45	∞	13.85	14.15
4171.32	1.00	0.12	SiIV 1402	0.262						
z = 1.8143										
4357.14	1.19	0.10	CIV 1548	0.194	65	14.1	60	∞	14.0	14.4
4364.21	0.73	0.10	CIV 1550	0.097						
Q 1101–264										
z = 1.8387										
3378.91	1.23	0.17	SiII 1190	0.251	55*	14.6				
3386.24	2.12	0.16	SiII 1193	0.500						
3578.03	1.97	0.11	SiII 1260	0.959						
4334.70	0.66	0.08	SiII 1526	0.076						
3956.39	1.11	0.05	SiIV 1393	0.528	30	14.1	25	40	13.7	14.2)
3981.95	0.83	0.05	SiIV 1402	0.262	6	17.4	0	6	17.4	17.5)
4394.71	1.37	0.07	CIV 1548	0.194	≳ 100	14.1	45	∞	14.1	14.3
4401.75	0.73	0.07	CIV 1550	0.097						
z = 1.4769										
3834.63	0.61	0.03	CIV 1548	0.194	≳ 60	13.7	60	∞	13.7	13.75
3840.87	0.26	0.03	CIV 1550	0.097						

* See text

7 Redshift distribution of absorption lines

If the absorbing material is cosmologically distant from and not closely associated with QSOs, then the number of absorption clouds seen in each QSO spectrum should in the absence of clustering have Poisson distribution. To test the distribution of absorption clouds it is important to make a distinction between the metal line systems which on this hypothesis would probably be associated with galaxies and hence may be expected to show some clustering, and the 'Lyα only' clouds which may be intergalactic (Arons 1972; Sargent *et al.* 1980). Typically only a few metal-lined systems are found in each QSO, so a large sample is required to study their distribution. The results of such a study have been reported by Weymann *et al.* (1979).

The distribution of the far more numerous Lyα only systems has been discussed in detail by Sargent *et al.* (1980). They have found that the degree of clustering of these clouds in the spectra of individual QSOs is minimal over a large range of scale lengths, and hence the cloud distribution should be close to Poissonian. In addition they show that the number of Lyα absorptions increases approximately exponentially as rest equivalent width decreases. It is thus critically important to set a lower bound on the rest equivalent width of lines considered in the sample, such that all lines of $W^r > W^r_{\rm min}$ should be observable anywhere within the Lyα sample wavelength range, provided they are not lost in blends. The value of $W^r_{\rm min} =$ 0.32 Å chosen by Sargent *et al.* (1980) is found to be adequate for our observations of Q0122 – 380 and Q1101 – 264 since our slightly lower effective resolution is compensated for by the substantially higher signal-to-noise ratio.

To estimate the density of Lyα absorption lines as a function of absorption redshift, $N(z)$, Sargent *et al.* (1980, section IIIc) have described a technique where the line samples from all QSOs at each z_{abs} are considered together. This may be visualized as a limiting case of counting the average number of absorption lines in wavelength (or redshift) bins over the total range available; see Weymann (1980), and then fitting a power law of the form $N(z) \propto (1+z)^{\gamma}$. For the seven QSOs we find $\gamma = 0.6 \pm 0.6$. Since we have added little to the Sargent *et al.* (1980) sample, our agreement with their estimate ($\gamma = 0.5 \pm 0.5$) is to be expected. Note, for comparison, that the dependence of N on z in the case where there is a constant co-moving density of clouds at cosmological distances from the QSO, is $N = N_0(1+z)(1+2q_0 z)^{-1/2}$, where N_0 is the (extrapolated) zero redshift value of $N(z)$.

A somewhat different method was used by Peterson (1978), in an analysis which did not take account of some of the selection effects discussed by Sargent *et al.* (1980). In applying this here for each QSO separately we determine one number, $\bar{N}$(QSO), the mean line density per unit absorption redshift. With each $\bar{N}$(QSO) we associate a value $\bar{z}_{abs}$, which is the mean absorption redshift in the Lyα sample window (*not* mean z_{abs} of observed lines); in this way $\bar{N}$ is a function of $\bar{z}_{abs}$. Values of $\bar{N}$ for the five QSOs discussed by Sargent *et al.* (1980) and the two reported in this paper are shown against $\bar{z}_{abs}$ in Fig. 3. Table 8 gives $\bar{N}$, $\bar{z}$ and N_0 values for these objects. We ask if the $\bar{N}$ values vary systematically with the mean absorption redshift, $\bar{z}_{abs}$, for the wavelength region sampled in each QSO. A fit to the function $\bar{N}(\bar{z}) \propto (1+\bar{z})^{\gamma}$ gives $\gamma = 1.4 \pm 0.7\,(1\sigma)$.

(Note that the mean value of N_0 for the two new objects is 16.1 ± 3.3 for $q_0 = 0$, and 27.8 ± 5.7 for $q_0 = ½$. These are in excellent agreement with the values of N_0 determined by Sargent *et al.* (1980) 17.7 ± 1.3 and 32.7 ± 2.4.)

A third possible method is to determine values for γ, as defined by the functional form above, separately for each QSO using the line wavelengths. This is similar to the first method, now applied individually to each QSO. The range of absorption redshifts and the number of lines observed are generally too small to allow γ to be well determined for each QSO. However, the weighted mean gives $\gamma = -2.1 \pm 1.5\,(1\sigma)$; suggesting more clouds at lower redshifts in contrast to the previous method. Table 9 sets the γ values for the individual QSOs. The same trend in line density is also apparent if $N(z)$ is plotted as a function of velocity relative to the QSO (Sargent *et al.* 1980, *V* and fig. 3).

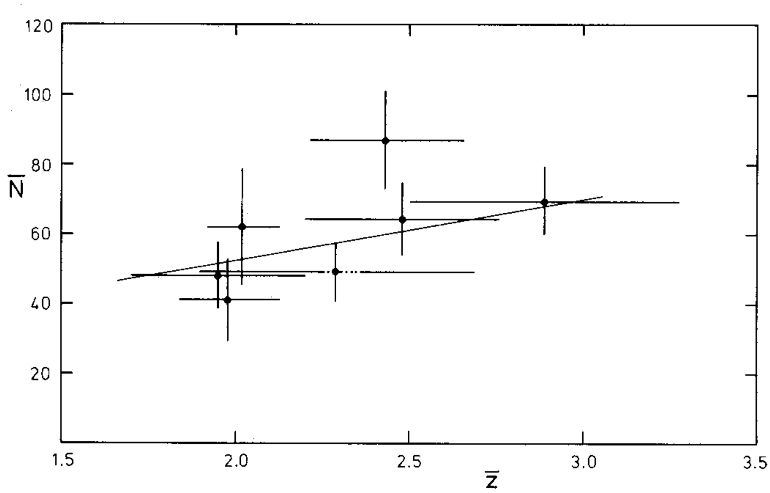

Figure 3. The redshift dependence of the absorption line density per unit redshift $\bar{N}$, for lines with rest equivalent width $\geqslant 0.32$ Å. The vertical error bars shown correspond to 1σ, and the horizontal lines indicate the redshift range used to determine the line densities. The region omitted from PHL 957 because of the strong Lyα in the $z_{abs} = 2.3085$ system is indicated by a dotted line. A best fit to the data for $N(z) \propto (1+z)$ (i.e. $q_0 = 0$ model) is also shown. The models for $q_0 > 0$ have flatter slopes and yield marginally worse fits to the data (see Table 8). The difference is totally insignificant, for the reasons discussed in the text.

Table 8. Mean Lyα line density for rest EW $\gtrsim 0.32$ Å.

QSO	z_{em}	Wavelength Range (A)	$\bar{z}$	Δz	No. lines	$\bar{N}$	$N_o(q_o=0)$	$N_o(q_o=\frac{1}{2})$
Q1101-264	2.14	3450 - 3800	1.98	0.29	12	41 ± 12	13.8 ± 40	23.8 ± 7.0
Q0122-380	2.18	3550 - 3800	2.02	0.21	13	62 ± 17	20.5 ± 5.6	35.7 ± 9.8
B2.1225+31.7	2.20	3282 - 3890	1.95	0.50	24	48 ± 10	16.3 ± 3.3	27.9 ± 5.7
Q0453-423	2.66	3902 - 4445	2.43	0.45	39	87 ± 14	25.3 ± 4.1	46.8 ± 7.5
PHL 957*	2.69	3525 - 4486	2.29	0.69	34	49 ± 8	15.0 ± 2.6	27.2 ± 4.6
Q0002-422	2.76	3890 - 4575	2.48	0.56	36	64 ± 11	18.5 ± 3.1	34.5 ± 5.7
Pks 2126-15	3.28	4255 - 5203	2.89	0.78	54	69 ± 9	17.8 ± 2.4	35.1 ± 4.8
Mean						58 ± 4	17.5 ± 1.2	32.0 ± 2.2
χ^2_6 (observed)						10.4	5.9	7.6

$\chi^2_6(0.95) = 12.6$
(theoretical)
$\chi^2_6(0.75) = 7.8$

*The entry for PHL 957 in Sargent et al. (1980), table 9, has been corrected here to allow for the strong Lyα at $z_{abs} = 2.3085$, which effectively removes about 120A from the wavelength range available for study. Sargent et al allowed for this in their analysis.

$\bar{N} = N_o\,(1+z)\,(1+2q_oz)^{-\frac{1}{2}}$, $\Lambda = 0$, where N_o is the inferred local ($z = 0$) line density per unit redshift.

Table 9. Redshift dependence of absorption line density in individual QSO spectra.

Object	Redshift range	γ *
Q1101-264	1.84 - 2.13	-7 ± 10
Q0122-380	1.92 - 2.13	23 ± 15
B2 1225+31.7	1.70 - 2.20	-3.8 ± 4.2
Q0453-423	2.21 - 2.66	-2.2 ± 4.3
PHL 957	1.90 - 2.69	-3.8 ± 4.0
Q0002-422	2.20 - 2.76	-3.9 ± 3.6
Pks2126-15	2.50 - 3.28	-0.5 ± 2.3
	Mean	-2.1 ± 1.5

* It is assumed that for each QSO the number of lines per unit redshift, $N(z) \propto (1+z)^{\gamma}$. Error estimates were determined from extensive Monte-Carlo simulation.

Why are the values of γ determined from the same raw data in these three different ways so disparate after we have gone to considerable trouble to ensure that the sample is free from redshift-dependent selection effects? One possibility is that the absorption line density does tend to increase with decreasing wavelength along a QSO spectrum, and the mean line density increases with QSO redshift. If this is true, then it is difficult to understand how most of the absorbing clouds could be at cosmological distances from, and unconnected with, the QSOs. However, it is well worth investigating in detail if there is some systematic effect hidden in the line selection procedures.

One possibility is that the presence of Lyβ at short wavelengths increases the apparent line density there. This should not affect our results, since only very short wavelength regions where this is possible have been included in the analysis, and any correction term appears to be small.

A further possibility is that line blending and uncertain continuum estimation affect the absorption line sample. It is possible, for example, that as the signal-to-noise ratio varies along a spectrum, or from spectrum to spectrum, blended lines may not be resolved and so weaker pairs or groups of lines be erroneously included. This is being investigated further.

Finally we point out that the number of objects is small. Confirmation (or otherwise) from an independent sample is highly desirable.

8 Conclusions

From the absorption and emission-line spectra of two QSOs, Q0122 – 380 (z_{em} = 2.181) and Q1101 – 264 (z_{em} = 2.143) we find:

(i) Weak but definite unidentified emission lines are present in both spectra, at λ1427 (in Q1101 – 264) and λ1120 (in Q0122 – 380).

(ii) Complex absorption redshift systems are present in the spectrum of Q0122 – 380, with one, at $z_{abs} = 1.97$, having components with a total spread in velocity perhaps as high as 1500 km s^{-1}. One of the systems in this complex shows possible N V absorption lines. N V lines have been reported in sharp-lined systems with redshifts very different from the QSO in only one other object, 4C05.34 (Coleman 1978), but are a common feature of broad-lined, probably ejected, systems. It is possible that the $z_{abs} = 1.97$ complex is an example of one of these in which condensations have formed, but it is also consistent with an intervening cluster of galaxies with velocity dispersion ~ 650 km s^{-1}.

(iii) Uncertain continuum determination can affect our measures of absorption line densities. If there are any systematic differences in such line densities with wavelength (or redshift), these could be masked by such uncertainties.

(iv) In individual QSOs the line density tends to decrease with increasing redshift, while for the sample of QSOs as a whole there is a small net increase with redshift. We stress that the sample size is still small. Also new selection effects which need to be investigated may account for the difference.

None the less, the very good agreement between the extrapolated values for the local space density of absorbers obtained for the two QSOs reported here and from the Sargent *et al.* (1980) sample of five is a further institute indication that there are no systematic differences between QSOs.

Acknowledgments

We are grateful to Bruce Peterson and Wal Sargent for a number of illuminating discussions on the interpretation of QSO absorption line counts, and the AAO staff for their usual efficient help in acquiring the observational data. RFC and DRI are grateful to the SRC for support.

References

Arons, J., 1972. *Astrophys. J.*, **172**, 553.
Bahcall, J. N., 1968. *Astrophys. J.*, **153**, 679.
Baldwin, J. A. & Netzer, H., 1978. *Astrophys. J.*, **226**, 1.

Boksenberg, A., Carswell, R. F. & Sargent, W. L. W., 1979. *Astrophys. J.*, **227**, 370.
Boksenberg, A., Carswell, R. F., Smith, M. G. & Whelan, J. A. J., 1978. *Mon. Not. R. astr. Soc.*, **184**, 773.
Boksenberg, A, and Sargent, W. L. W., 1975. *Astrophys. J.*, **198**, 31.
Carswell, R. F., Smith, M. G. & Whelan, J. A. J., 1977. *Astrophys. J.*, **216**, 351.
Chan, Y. W. T. & Burbidge, E. M., 1971. *Astrophys. J.*, **167**, 213.
Coleman, G., 1978. *PhD Thesis*, University of Arizona.
Coleman, G., Carswell, R. F., Strittmatter, P. A., Williams, R. E., Baldwin, J., Robinson, L. B. & Wampler, E. J., 1976. *Astrophys. J.*, **207**, 1.
Lynds, C. R., 1971. *Astrophys. J.*, **164**, L73.
Morton, D. C., 1978. *Astrophys. J.*, **222**, 863.
Morton, D. C. & Richstone, D. O., 1973. *Astrophys. J.*, **184**, 65.
Morton, D. C., Chen, Jiang-Shen, Wright, A. E., Peterson, B. A. & Jauncey, D. L., 1980. *Mon. Not. R. astr. Soc.*, **193**, 399.
Morton, W. A. & Morton, D. C., 1972. *Astrophys. J.*, **178**, 607.
Oke, J. B., 1974. *Astrophys. J. Suppl.*, **27**, 21.
Osmer, P. S. & Smith, M. G., 1977a. *Astrophys. J.*, **213**, 607.
Osmer, P. S. & Smith, M. G., 1977b. *Astrophys. J.*, **215**. L47.
Peterson, B. A., 1978. In *The Large Scale Structure of the Universe: IAU Symp. No. 79*, p. 389, ed. Longair, M. S. & Einasto, J., D. Reidel, Dordrecht.
Sargent, W. L. W., Young, P. J., Boksenberg, A., Carswell, R. F. & Whelan, J. A. J., 1979. *Astrophys. J.*, **230**, 49.
Sargent, W. L. W., Young, P. J., Boksenberg, A. & Tytler, D., 1980. *Astrophys. J. Suppl.*, **42**, 41.
Smith, M. G., 1975. *Astrophys. J.*, **202**, 591.
Smith, M. G., 1976. *Astrophys. J.*, **206**, L125.
Smith, M. G., 1978. *Vistas Astr.*, **22**, 321.
Smith, M. G., Carswell, R. F., Whelan, J. A. J., Wilkes, B. J., Boksenberg, A., Clowes, R. G., Savage, S., Cannon, R. D. & Wall, J. V., 1981. *Mon. Not. R. astr. Soc.*, **195**, 437.
Strömgren, B., 1948. *Astrophys. J.*, **108**, 242.
Weymann, R. J., 1980. *Phil. Trans. R. Soc. Lond.*, **A 296**, 399.
Weymann, R. J., Williams, R. E., Peterson, B. M. & Turnshek, D. A., 1979. *Astrophys. J.*, **234**, 33.
Whelan, J. A. J., Smith, M. G. & Carswell, R. F., 1979. *Mon. Not. R. astr. Soc.*, **189**, 363.
Williams, R. E., Strittmatter, P. A., Carswell, R. F. & Craine, E. R., 1975. *Astrophys. J.*, **202**, 296.
Wills, D. & Netzer, H., 1979. *Astrophys. J.*, **233**, 1.
Young, P. J., Sargent, W. L. W., Boksenberg, A., Carswell, R. F. & Whelan, J. A. J., 1979. *Astrophys. J.*, **229**, 891.